Defence Science Journal, Vol. 59, No. 4, July 2009, pp. 425-435

Swift Heavy Ion-induced Mixing

S.K. Srivastava[1] and D.K. Avasthi[2]
[1]*Indian Institute of Technology Kharagpur-721 302*
[2]*Inter-University Accelerator Centre, New Delhi-110 067*

ABSTRACT

In this paper, the possible swift heavy ion (SHI)-matter interaction processes and their applicability to SHI-induced mixing have been discussed. The assumption that the SHI mixing is a consequence of a transient molten state diffusion has been brought forward. The following experimental evidences have been presented to verify the concepts developed for SHI mixing process: (i) Evidence of high temperature conditions in materials produced by SHI's via the study of SHI mixing in an *Fe*/*Fe*^{57}/*Si* system; (ii) Verification of the hypothesis of transient molten state diffusion via a detailed study on *Fe*/*Si* system; (iii) The role played by a thermodynamical parameter, viz., interfacial free energy via a SHI mixing study on an *Fe*/*Si* multilayer; (iv) Demonstration of the occurrence of the process in an exclusively thermal-spike determined metal/metal system, viz., *Fe*/*Ni* multilayer; and (v) synthesis of technologically important *Si*C phases at room temperature via SHI mixing of C-allotrope/*Si* multilayers.

Keywords: Swift heavy ion (SHI), ion-beam mixing, thermal spike model, transient enhanced diffusion.

1. INTRODUCTION

Observation of defect production and atomic motion induced by swift heavy ions[1,2] has stimulated interest in achieving SHI-induced mixing at interfaces[3] to produce novel materials and phases since 1991. The cause of mixing is essentially a transfer of the energy deposited by the ions in the electronic subsystem to the lattice to cause atomic displacements. Two models, viz., the Coulomb spike model[4] (CSM) and the thermal spike model[5–7] (TSM), have been invoked to explain such atomic displacements. According to the CSM, a swift heavy ion while passing through a material medium causes ionisation of the medium around its path in a time scale of 10^{-17} s. This is followed by a strong electrostatic repulsion among these charges, taking place within 10^{-14}–10^{-13} s, which leads to a vivid atomic motion and results finally in a cylinder of modified material.

As far as insulators and most semiconductors are concerned, the life-time of the excited electrons, or in other words, the time of existence of the ionic state of matter, is long enough for the Coulomb explosions to take place. In metals, however, the high mobility of conduction electrons leads to the neutralisation of charges in a fraction of a femtosecond, much before the Coulomb explosion could occur[8], invalidating the applicability of the CSM in metals. The TSM, on the other hand, assumes that the energy deposited initially in the electronic subsystem in 10^{-15}–10^{-14} s gets subsequently transferred to the atomic subsystem via electron-phonon (*e-p*) coupling in 10^{-13}–10^{-12} s. This results in a rapid rise in the lattice temperature up to ~10^4 K (thermal spike). Above a certain threshold S_{eth} of electronic energy loss S_e, the material within a few nanometers from the ion path melts for a duration of 10^{-12}–10^{-11} s. The molten state then quenches at a very fast rate of 10^{14} K/ s, forming latent tracks. The TSM has a versatile applicability to all kinds of materials.

The explanation of SHI- induced mixing across interfaces by the CSM is described. When the projectile ion passes through the interface of two materials, which may have different dielectric constants, the cylindrical symmetry of the space charge, and hence of the electric field around the interface breaksdown, which may develop longitudinal components. This longitudinal component of the field may then mingle the atoms from two sides of the interface and a thin mixed zone is formed. Quantitative estimation of this effect is rather difficult, but the extent of mixing by this mechanism should be feeble, if at all it takes place. Moreover, the mechanism can be effective only in insulators; in case of any component being metallic, this mechanism does not apply.

The applicability of the thermal spike model to SHI mixing, on the other hand, lies in the fact that the ion creates a molten state of the material it traverses around its track. For whatsoever short duration (~1–100 ps) the molten state of the material may exist, it will be accompanied by diffusion-controlled motion of atoms in the liquid before it freezes in its finally-modified state. Now, if the sample under irradiation possesses an interface between two materials, it is anticipated that a transient (of thermal spike or molten state duration) liquid-state interdiffusion across the interface will take place in the latent track. The liquid state diffusivities are large (of the order of

Received 12 January 2009

10^{-9}–10^{-8} m^2/s), and hence can lead to an observable intermixing across the interface during even the short existence of the molten state of the latent tracks. The phenomenon should apply to all kinds of materials, which, with certain combination of ion species and ion energy (or S_e), can be modified by the swift heavy ions. Such materials are conventionally known as S_e-sensitive ones. Because of the large liquid state diffusivities, the amount of interface mixing taking place via this mechanism should be much higher than that via the Coulomb spike mechanism, even in the case of insulators or semiconductors; In case of metals, the latter mechanism anyway is ineffective. Thus, it is harmless to assume that SHI mixing is a consequence principally of a thermal-spike-model-based phenomenon. Our next strategy would be to verify this assumption, for which the most appropriate systems would be those having at least one metallic component, eliminating thereby any (feeble) possibility of Coulomb-spike driven contribution.

Although by now, a multitude of SHI mixing studies aimed primarily at achieving it in different combinations of binaries, and in some cases, at finding out or verifying the underlying mechanisms, have been reported, the present study has been done in a systematic manner. The authors aim first at verifying the assumptions of the applicability of the thermal spike model and the hypothesis of transient molten state diffusion in a well studied *Fe*/*Si* system, then attempt to mix a more difficult metal/metal system, and finally applying the knowledge gained in room temperature (RT) synthesis of a compound, viz., *SiC*, which otherwise is difficult to fabricate by conventional means.

2. EXPERIMENTAL

2.1 *Fe*/*Fe*^{57}/*Si* System: Evidence of High Temperature Conditions

In this study, conversion electron Mössbauer spectroscopy (CEMS) technique was employed to study the mixing induced by 175 MeV *Au* and 200 MeV *Ag* ions (delivered by the Pelletron at IUAC, New Delhi) at the *Fe*^{57}/*Si* interface in an *Fe*/*Fe*^{57}/*Si* system[9].

The CEMS spectra of the pristine sample and those of the samples irradiated at various fluences are shown in Fig. 1. Each spectrum is composed of a sharp sextet corresponding to α-*Fe*, and a paramagnetic doublet indicative of formation of iron silicide. A weak paramagnetic doublet in the CEMS spectrum of the pristine sample indicates that a small fraction of *Fe*^{57} has been mixed at the interface during the film deposition process itself, in agreement with a previous report[10,11]. This doublet, however, is broad and suggests that the mixed region of the pristine sample is amorphous in nature, unlike the cases of irradiated samples, where the doublets are sharp and the mixed phase can be identified. The formation of this crystalline mixed phase, thus, can solely be attributed to the phenomena taking place following the SHI irradiation. An analysis of the hyperfine parameters leads to the following inferences:

1. The unmixed part of the sample (corresponding to the sextets) remains α-*Fe*.

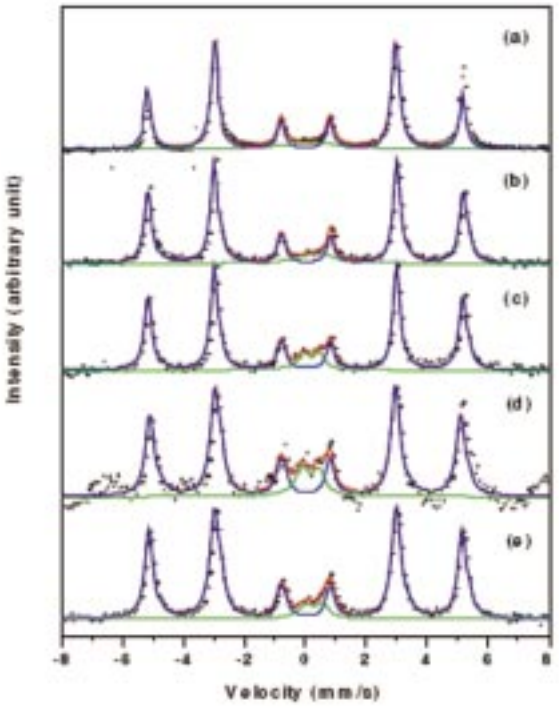

Figure 1. CEMS spectra of pristine (a) 175 MeV *Au* irradiated at 5.3×10^{11} ions/cm^2 (b) 4.4×10^{12} ions/cm^2 (c) 1.0×10^{13} ions/cm^2 (d) 200 MeV *Ag* irradiated at 1.0×10^{13} ions/cm^2 and (e) samples. The dots are the data, and the continuous lines are the corresponding fits.

2. On comparing the hyperfine parameters of doublets with those corresponding the five possible *Fe*-*Si* mixed phases, viz., α-Fe_3Si (sextet), α'-Fe_3Si (sextet), ε-*FeSi*, β-$FeSi_2$, and α-$FeSi_2$, the closest are those for α-$FeSi_2$.
3. The contribution of the mixed phase to the spectrum increases monotonically with ion fluence.
4. For the case of lower S_e value (175 MeV *Ag*), the amount of mixing is less.

The formation of α-$FeSi_2$ phase, which forms at temperatures above 937 °C and deviates from the stoichiometric composition with ~13 per cent vacancies, indicates that the ion creates a high temperature condition in the material and produces defects in it. This gives an evidence of the applicability of the thermal spike model to the case of SHI mixing. The S_e values involved are more than the S_{eth} in *Fe* and latent tracks are created around the ion path. Mixing of atoms across the interface takes place within these tracks. The average size of these tracks can be estimated from the variation of the fractional area *F* of the doublet, i.e., the fraction of *Fe*^{57} atoms mixed with *Si*, with ion fluence ϕ. The fraction *F* can be considered as the fraction of *Fe* atoms which were previously in a crystalline state and have been, due to irradiation effects, surrounded by *Si* atoms. If one assumes that the mixing takes place along the ion tracks of cross-sectional area $\sigma = \pi r^2$ (r = track radius), the rate of increase $dF/d\phi$ of the fraction *F* with ϕ will be proportional to σ and to the unmixed *Fe* fraction

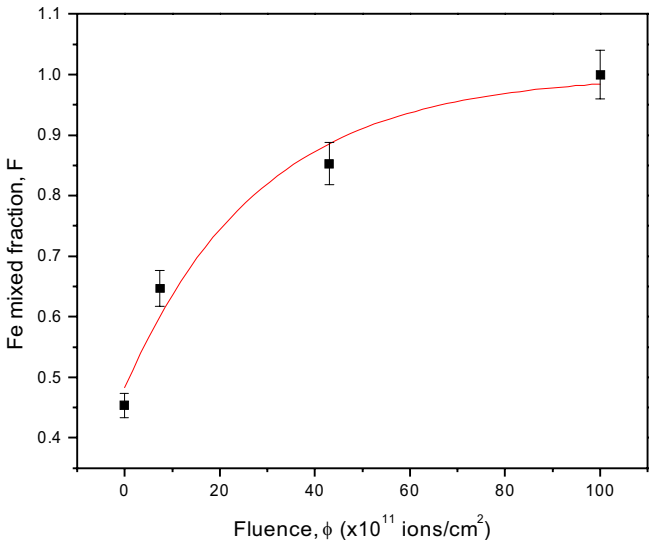

Figure 2. Plot of the fraction *F* versus ion fluence. The continuous line is an exponential fit to the data (dots).

(1–*F*). Thus

$$\frac{dF}{d\phi} = \sigma(1-F) \qquad (2)$$

Solving this equation yields

$$F = 1 - F_0 \exp(-\pi r^2 \phi) \qquad (3)$$

Here, F_0 is the fraction of *Fe* mixed during deposition. A plot of *F* versus ϕ is shown in Fig. 2, which, on fitting with Eqn. (2) yields an average ion track radius of ~3.3 nm. The fit to the curve gives $F_0 = 0.48$ and $\sigma = \pi r^2\phi = 3.5\times10^{-13}$ cm^2, which in turn gives the track radius as 3.3 nm.

The above study suggests that swift heavy ions(SHI) are capable of producing high temperature conditions in materials, and hence lend credence for the interface mixing process to the thermal spike model of defect creation.

2.2 *Fe*/*Si* System: Verification of the Hypothesis of Transient Molten State Diffusion

The motivation behind this work was to verify the *hypothesis* that the SHI mixing is a consequence of transient molten state diffusion via a careful study of 230 MeV *Au* ion-induced mixing at an *Fe* (59 nm)/*Si* interface, monitored online by elastic recoil detection analysis (ERDA) technique[12]. The ion beam was incident on the sample surface at a grazing angle of 10° and the *Fe* and *Si* recoil atoms, induced by the elastic-collisions taking place because of the finite (howsoever small) S_n values, were collected at a scattering angle of 37.5° in a large-area position sensitive detector telescope. Two energy signals – Δ*E* and *E* – generated by the recoils in two separate sections of the detector telescope, were recorded to generate a two-dimensional Δ*E*-*E* spectrum, which exhibits different spectral bands for different elements. From the two-dimensional spectrum, regions corresponding to *Si* and *Fe* recoils were selected and projected onto *E* axis to obtain one-dimensional *Si* and *Fe* recoil energy spectra. The data were collected in list mode and were later divided into equal parts, each having an ion fluence of 8.75×10^{13} ions/cm^2, to get the recoil energy spectra at different fluences. The authors strategy to verify the hypothesis was to determine the presumed diffusion coefficients experimentally, and compare them with the standard, literature values of liquid-state diffusivities. The requirements now for the estimation of the diffusivities are the interdiffusion profiles of *Fe* and *Si* near interface, which should be derivable from the experimental data, and the appropriate diffusion time.

The ion fluence-dependent interdiffusion profiles were obtained by fitting the ERDA spectra using the code SIMNRA[13]. In the fittings, a surface roughness of 3 nm, based on an atomic force microscopy (AFM) study on the same set of samples with similar irradiation conditions, was taken as an input parameter. The *Fe* and *Si* recoil energy spectra in the interfacial region, along with the corresponding SIMNRA fits, for four different ion fluences are shown in Fig. 3. The concentration versus depth profiles of *Fe* derived from the SIMNRA fits were plotted in the inset, which show a monotonic increase in the amount of intermixing (interdiffusion) with increasing fluence.

Here, it would be appropriate to address another issue: It has so far been argued that the S_e in *Fe* being more than the corresponding S_{eth}, *Fe* should melt; but what happens to the material on the other side of the interface, i.e., to *Si*, when it is known that monatomic swift heavy ions do not produce modifications[14] in bulk *Si*. For the hypothesis to be valid at the first place, it is necessary that *Si* also melts to facilitate liquid state diffusion. Here, actually what one requires is the melting of *Si* merely at the interface; the absence of any SHI- induced modification of the bulk of the *Si* substrate becomes

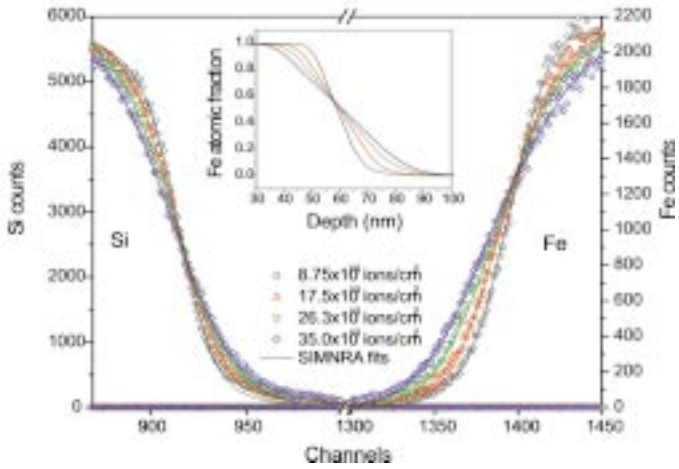

Figure 3. The interfacial edges of the recoil energy spectra (symbols) and the corresponding SIMNRA fits (continuous lines) for four fluences. The inset shows the depth profiles of the *Fe* atomic fraction for the four fluences as derived from the SIMNRA fits.

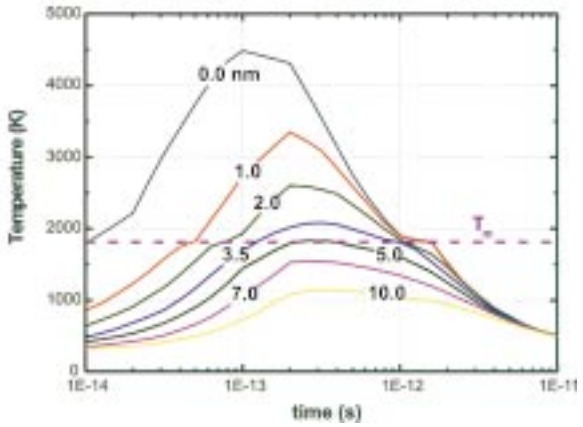

Figure 4. Evolution of *Fe* lattice temperature with time for various radii *r* of cylinders around a 230 MeV *Au* ion path as calculated using the thermal spike model. A horizontal line depicting the *Fe* melting temperature T_m is also shown.

immaterial. At this instance, a thermal-spike-model calculation by Wang,[15] *et al.* for SHI effects at *Si* surface and interface comes to rescue. They tried to calculate the temperature evolution of *Si* to describe the surface-or interface-defect creation and conclude that with a beam energy of 0.05 MeV/u, melting of *Si* close to the surface or interface should appear above an S_e of 6 keV/nm. The reason for the lack of observation of any SHI induced modification in bulk *Si* using monatomic ions could be the rapid reconstruction of *Si-Si* bonds[16]. Thus, one can safely assume that *Si* also melts near the interface, for the present S_e (~ 17.1 keV/nm) in *Si* is more than the calculated threshold (~ 6 keV/nm).

Now since the presumed diffusion takes place in the transient liquid state created by the thermal spike, one needs to perform the thermal spike calculation to see the evolution of *Fe* lattice temperature with time for a number of cylinders of different radii around the path of a 230 MeV *Au* ion at normal incidence. The result of this calculation is shown in Fig. 4.

It can be observed from the Fig. 4 that up to 4 nm of cylinder around the ion path remains at or above the melting temperature for at least 1.2 ps. For computational simplicity, these values in *Fe* can be taken as the molten track radius *r* and spike time t_s, respectively, in all molten regions. The diffusion time *t* is calculated based on the following considerations.

At a particular fluence ϕ_s, the ion irradiated spot is filled up with tracks, each of radius *r*.

The diffusion time for each fluence step would be the duration of the molten phase t_s. Since the recoils are produced in a typical ion-matter interaction time of ~ 10^{-17} s, an event taking place much earlier than lattice modification (~ 10^{-12} s), those from the very first ϕ_s fluence do not probe any lattice modification. The recoils from the second ϕ_s fluence, however, encounter the modified lattice (the modification has occurred during time t_s in the first ϕ_s fluence). Thus, for a fluence ϕ, the time of diffusion is

$$t = (\phi/\phi_s - 1)\, t_s \quad = \quad (\pi r^2 \phi - 1)\, t_s \tag{4}$$

The next step was to use the diffusion profiles for calculating (fluence-dependent) diffusivities. Since the diffusion in this case is a kind of interdiffusion (of *Fe* and *Si* across the interface) and not of impurity diffusion, the diffusion coefficient becomes concentration- dependent and Matano analysis[17] of the derived concentration versus depth profiles (Fig. 3) is required for its estimation. Diffusivities of *Fe* in *Si* and vice versa so obtained were then compared with the known results.

An important point to be considered here is the oblique incidence angle α (= 10° from the sample surface) of the ions. It has two effects:

(i) The interface area affected by a track increases by a factor of $(\sin \alpha)^{-1}$;

(ii) the cylindrical symmetry of the energy transfer around the ion path is broken in the vicinity of the interface.

The lattice, in this case, acquires higher temperatures for longer duration than those derived from the thermal spike model calculations, causing larger atomic displacements. The observed amount of intermixing, or equivalently, the diffusion length $L_{obs} = (2D_{obs}\, t)^{1/2}$, where D_{obs} is the observed diffusivity and *t* is the diffusion time, then, becomes proportional to $(\sin \alpha)^{-n}$ with $n>1$. From sputtering of solid oxygen[18], LiF[7], and SiO_2 [19], where the relevant quantity -the volume of the material inside a track-increases by a factor of $(\sin \alpha)^{-1}$, it has been shown that the sputtering yield is proportional to ~ $(\sin \alpha)^{-1.7}$. For the present case also, the same angular dependence can be assumed. Thus, the actual diffusivity *D* should be equal to $(\sin \alpha)^{3.4} \times D_{obs}$.

According to the Matano method (Fig. 5), including the angular dependence, the interdiffusion coefficient $D(c)$ at an atomic concentration *c* at a distance *x* is determined by the inverse of the slope $|\partial x/\partial c|_c$ of the concentration versus depth curve at the same concentration and the area $\int_0^c x\, dc'$ between the curve up to the concentration *c* and the Matano plane, is defined by (Fig. 5).The Matano plane is defined by a vertical line which renders the area A equal to the area B. The diffusion coefficient at a concentration *c* is determined by the tangent at the point c and by the area enclosed by the Matano plane, the horizontal line at *c*, the depth profile and the x-axis.

$$\int_0^1 x\, dc' = 0 \tag{5}$$

and is given by

$$D(c) = (\sin \alpha)^{3.4} \frac{1}{2t} \left.\frac{\partial x}{\partial c}\right|_c \int_0^c x\, dc' \tag{6}$$

The concentration-dependent interdiffusion coefficients thus calculated for the four analysed fluences have been plotted in Fig. 6. The intrinsic diffusivities D_I of *Fe* in *Si* and D_{II} of *Si* in *Fe* can be taken as the values of interdiffusion coefficients in the limit of infinite dilution. The two diffusivities, taking into account the contribution

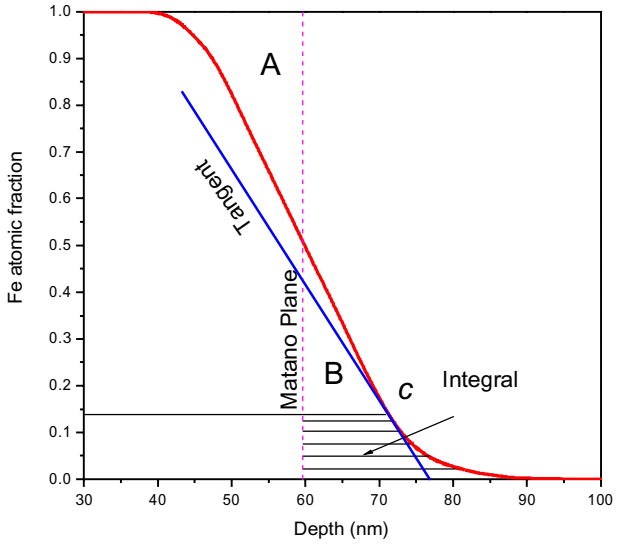

Figure 5. Schematic illustration of the Matano analysis of *Fe* atomic fraction versus depth profile.

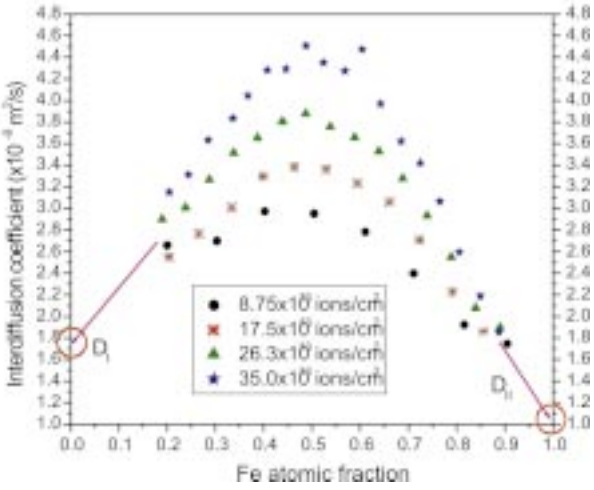

Figure 6. Plots of interdiffusion coefficient against *Fe* atomic fraction as obtained from the Matano analysis of the depth profiles of the latter for the four ion fluences.

of errors from the fluence calculation (~ 20%), energy resolution of the detector (~ 1%), ion incidence angle (~ 1%), and stopping power (~ 20%), are $(1.1\pm0.4)\times10^{-9}$ and $(5.1\pm 2.0)\times10^{-10}$ m^2/s, respectively.

These values are close to (only about an order of magnitude less than) the literature values of diffusivities in liquid metals[20] and liquid[21] *Si*. The observed difference is typical for a liquid in contact with a solid surface – the viscous drag of the melts along the track wall retards the atomic mobility and consequently the diffusivity. The corresponding solid state diffusivities even at melting temperatures[22] are 3.0×10^{-11} and 1.0×10^{-11} m^2/s , respectively – about two orders of magnitude less than the observed diffusivities. Therefore, the possibility of solid state diffusion is ruled out. The hypothesis that the SHI mixing is a consequence of a transient molten state diffusion is, thus, verified.

2.3 *Fe*/*Si* Multilayer: Effect of Interfacial Free Energy on SHI Mixing

Having established that the SHI mixing mechanism is based on a thermal process (thermal spike), it would be interesting to see how some other thermodynamical parameters, e.g., interfacial Gibbs free energy, can affect the SHI mixing process. Depending on the miscibility and occurrence of intermetallic phases, the Gibbs free energy of a compound of *A* and *B* may be above or below the line joining the free energies of the pure constituents. Figure 7 (a) is an illustrative Gibbs free energy diagram, the line emanating from G_i (i.e. the zero line) being the composition-dependent free energy curve for a mechanical mixture.

To achieve a mixed phase/compound of composition F, one would need to provide the difference $\Delta G = G_i - G_F$ in the free energy by some means; in case of SHI mixing, it is the energy deposition by the ions which provides this

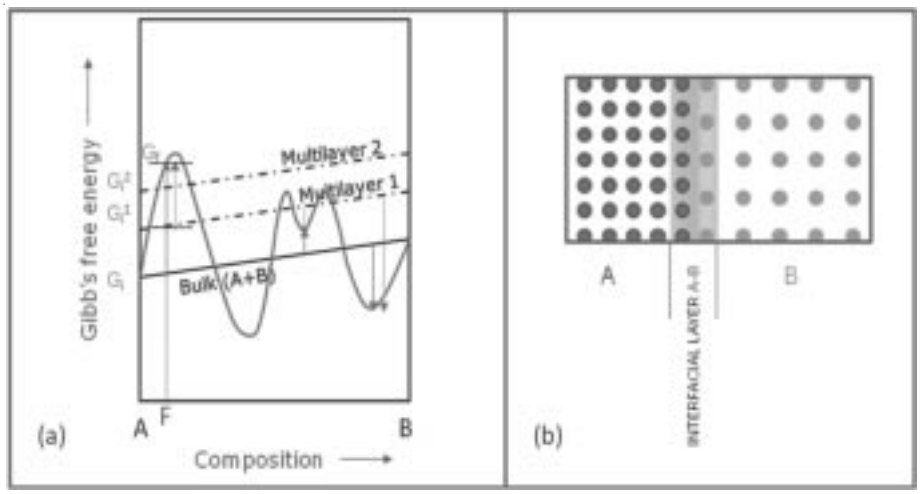

Figure 7. (a) A schematic of a general free energy versus binary composition diagram. (b) Another schematic showing the interface layer containing the metastable configuration of atoms around an interface.

driving thermal force. If there are interfaces present – e.g., in a thin-film/substrate couple or in a multilayer – between elemental materials A and B, the atoms in the interfacial regions are in a metastable configuration Figure 7 (b). The interfaces have been confirmed to be in a disordered state by X-ray diffraction analysis[23,24]. Consequently, the interfacial free energies of all the interfaces get added to the zero line, and the Gibbs free energy of the initial state of the A-B multilayered films gets elevated by an amount equal to the total interfacial free energy. This elevation of the zero line reduces the required driving force ΔG of mixing. Furthermore, the fraction f of the interfacial atoms versus the total atoms in the multilayer is proportional to the number of interfaces divided by the total multilayer thickness. Thus, two multilayers ML_1 and ML_2 with interfacial fractions f_1 and f_2 ($f_1 < f_2$) will have their initial free energies elevated to G_{i1} and G_{i2} ($G_{i1} < G_{i2}$), respectively. It would then be easier to mix ML_2 than ML_1.

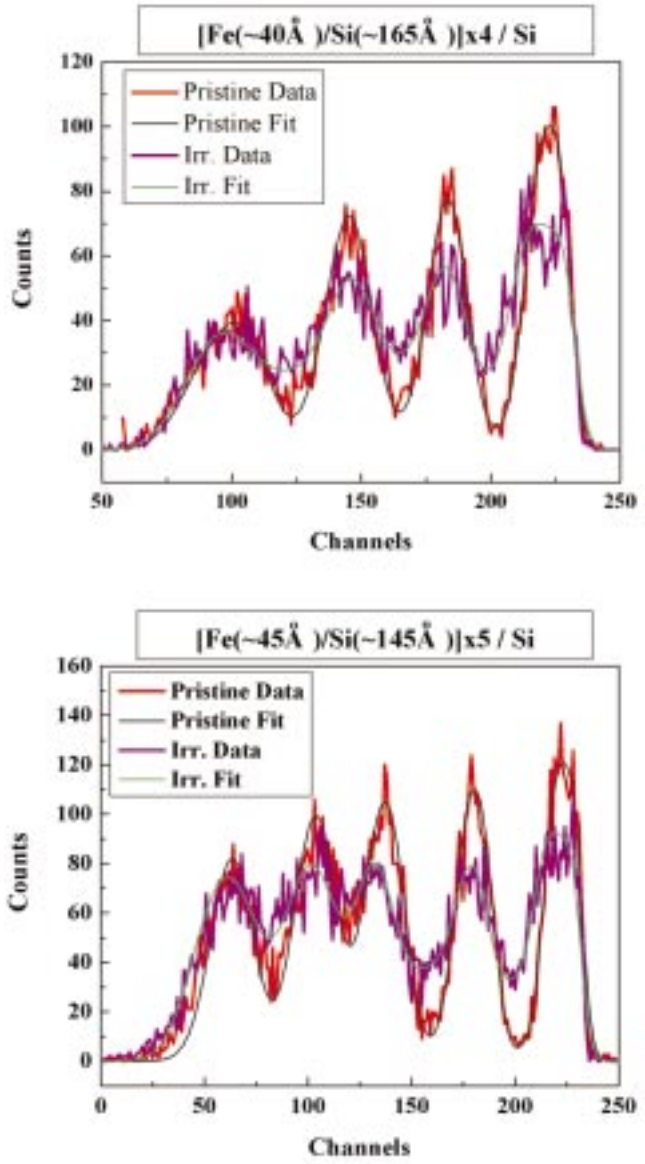

Figure 8. The HRBS data and corresponding SIMNRA fits of pristine and 4.2×10^{13} ions/cm^2, 350 MeV *Au* irradiated (a) ML_1 and (b) ML_2 multilayers.

Based on these considerations, two *Fe*/*Si* multilayers – ML_1: [*Fe* (40 Å) / *Si* (165 Å)]×4 and ML_2: [*Fe* (45 Å) / *Si* (145 Å)]×5 –were deposited on *Si* substrates and were irradiated them with 350 MeV Au ions at 4.2×10^{13} ions/cm^2 fluence. The corresponding f values are proportional to [7/(40+165)×4] = 0.085 and [9/(45+145)×5] = 0.095, respectively and differ by ~ 10 per cent. The S_e exceeds the threshold of 30 keV/nm and the S_n is insignificant to affect the mixing process. The pristine and irradiated samples were characterized by High-resolution Rutherford Backscattering Spectrometry (HRBS) The HRBS spectra were fitted using the code SIMNRA. The spectra for the two multilayers, and their fits, are shown in Fig. 8. The channels on the abscissa represent the depth starting from the rightmost edge, and the counts on the ordinate represent the fractional amount of *Fe* (wrt to the amount of *Si*). The interdiffusion/mixing of *Fe* atoms (peaks) into *Si* layers (valleys) is clearly evident from the figure.

Table 1. The differences for the interfacial fraction f and amounts of and 4.2×10^{13} ions/cm^2, 350 MeV *Au* induced mixing in the *Fe*/*Si* multilayers

Observable	ML_1	ML_2	Percentage difference
f	∝ 7/(205x4)	∝ 9/(190x5)	~10.0
Fe in *Si* layer (after irradiation)	~0.16	~0.20	~25.0
Si in *Fe* layer (after irradiation)	~0.32	~0.40	~25.0

The SIMNRA-fit determined compositions of the samples after irradiation are ~[$Fe_{0.68}Si_{0.32}/Fe_{0.16}Si_{0.84}$]×4 and ~[$Fe_{0.60}Si_{0.40}$ / $Fe_{0.20}Si_{0.80}$]×5 for ML_1 and ML_2, respectively. Table 1 highlights the difference between the amounts of mixing in ML_1 and ML_2.

The significantly higher amount of mixing, as described in the Table, for ML_2 (larger interfacial free energy) than for ML_1, suggests that the thermodynamic parameter, viz., the interfacial free energy plays an important role in SHI mixing process, approving the assumption of the applicability of the thermal spike model in the process.

2.4 *Fe*/*Ni* Multilayer: SHI Mixing in a Metal/Metal System

Having gained the confidence that the SHI mixing mechanism is a thermal-spike-based phenomenon, it is imperative to explore the possibility of the process in a metal/metal system, wherein it is the thermal spike model which is valid exclusively. This idea was enacted via the observation of effect of 120 MeV Au ion irradiation of *Fe*/*Ni* multilayers of structure [*Ni* (13 Å)/*Fe* (33 Å)]×10. The multilayers were irradiated at 1×10^{13} ions/cm^2 and 1×10^{14} ions/cm^2 fluences. The S_e was above S_{eth} and the S_n was

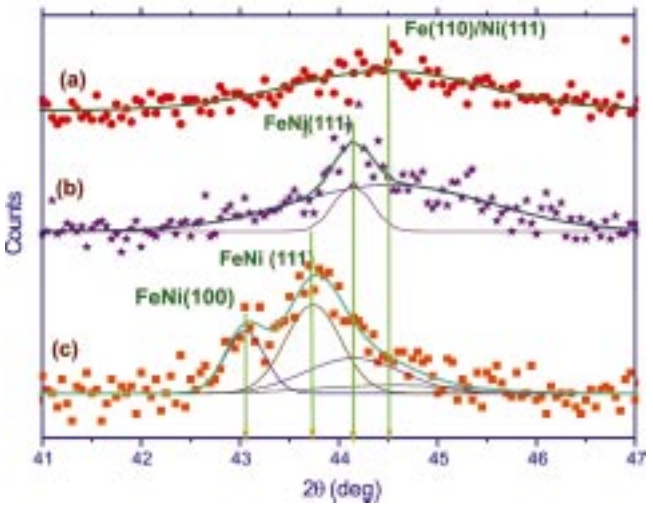

Figure 9. XRD spectra of (a) pristine, (b) irradiated at 1×10^{13} ions/cm^2 and (c) irradiated at 1×10^{14} ions/cm^2 *Fe*/*Ni* multilayers. The lines are Gaussian fits and fit components.

insignificant. The pristine and irradiated samples were characterised by X-ray diffraction (XRD), electrical resistivity, X-ray reflectivity and Magneto-optical Kerr effect, results of the first two of which are discussed here. Detailed discussion including the results from the last two techniques can be found elsewhere[25].

The XRD spectra in the range 41° d_∞ 2θ d_∞ 47° and the Gaussian fits to the possible peaks for the pristine and irradiated samples are shown in Fig. 9. The spectrum for the pristine sample consists only of a single broad peak of width 2.72° centered at 44.48°. *Si*nce *Fe*(100) (2θ = 44.67°) and *Ni*(111) (2θ = 44.51°) reflections occur at almost the same place, this peak can be considered as the *Fe*/*Ni* system peak. After irradiation at 1×10^{13} ions/cm^2 fluence, a new sharp (width = 0.38°) peak develops at 44.14°, which corresponds to the (111) plane of ferromagnetic $FeNi_3$ phase. This new phase formation is a clear evidence of SHI mixing in the *Fe*/*Ni* multilayer. After augmenting the irradiation to 1×10^{14} ions/cm^2 fluence, two new peaks emerge at 43.74° and 43.05°. These peaks, which constitute ~65% of the total XRD spectrum area, can be indexed as *FeNi*(111) and *FeNi*(100), respectively. The $FeNi_3$(111) peak still exists and covers ~30% of the total area. The broad system peak has almost vanished (<10%), showing an almost complete mixing of the multilayer at this fluence.

Figure 10 shows the plot of room temperature resistivity versus ion fluence. From the plot, it can be noted that the resistivity ρ_{prist} of the pristine sample is unusually high –104 μΩ-cm against the low bulk resistivities ρ, *Fe* = 9.8 μΩ-cm and ρ_∞,*Ni* = 7.2 μΩ-cm of the constituents *Fe* and *Ni*, respectively. One would, in fact, have expected the resistivity to be between the two bulk values. The explanation of the anomaly has to be sought in the structure of the multilayer. The resistivity of the multilayer originates from

(i) The isotropic background scattering due to the combined effects of phonons, magnons and the defects and impurities present in the sample,
(ii) The scattering due to the grain boundaries, and
(iii) The scattering due to surfaces and interfaces.

The first two contributions constitute the intrinsic resistivity ρ_{Int}. According to the Fuchs size-effect theory[26], the intrinsic scattering mechanisms carry over to the film; in addition, the interfaces impose a boundary condition on the electron transport. According to Mayadas and Shatzkes[27], the resistivity of a single layer of a multilayer is determined by the following set of equations:

$$\frac{\rho_\infty}{\rho_{Int}} = 3\left[\frac{1}{3}-\frac{1}{2}\beta+\beta^2-\beta^3\ln\left(1+\frac{1}{\beta}\right)\right] \tag{7}$$

$$\beta = \frac{\lambda_\infty}{D}\frac{R}{1-R} \tag{8}$$

$$\frac{\rho}{\rho_\infty} = \left[\frac{\rho_\infty}{\rho_{Int}} - \frac{6}{\pi\kappa}(1-p)\times\int_0^{\pi/2} d\phi\times\int_1^\infty dt\,\frac{\cos^2\phi}{H^2(t,\phi)}\right.$$
$$\left.\times\left(\frac{1}{t^3}-\frac{1}{t^5}\right)\frac{1-e^{-\kappa t H(t,\phi)}}{1-pe^{-\kappa t H(t,\phi)}}\right]^{-1} \tag{9}$$

$$H(t,\phi) = 1+\frac{\beta}{\cos\phi\times\left(1-\frac{1}{t^2}\right)^{1/2}} \tag{10}$$

Here, ρ_∞ is the bulk resistivity; ρ_{Int}, the intrinsic resistivity; λ_∞, the electron mean free path in bulk; *D*, the average grain diameter; *R*, a reflection coefficient characteristic of the grain boundaries and defects, and $0 \le p \le 1$ is a specularity parameter appropriate for electron scatterings from layer interfaces. The parameter *p* is equal to 1 for a sharp interface and 0 for a rough interface; see Figure 25. Once the resistivities ρ_j of the individual layers *j* are determined, and if the thickness d_j of the j^{th} layer is less than the electron mean free path in the corresponding bulk, the multilayer resistivity ρ_M can be obtained by[28]

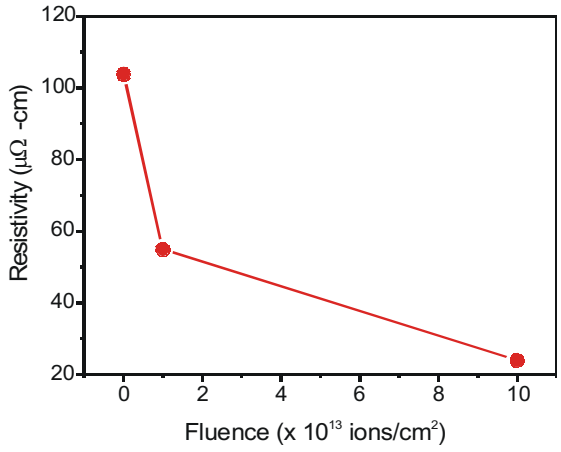

Figure 10. The plot of RT resistivity versus ion fluence for the *Fe*/*Ni* multilayers.

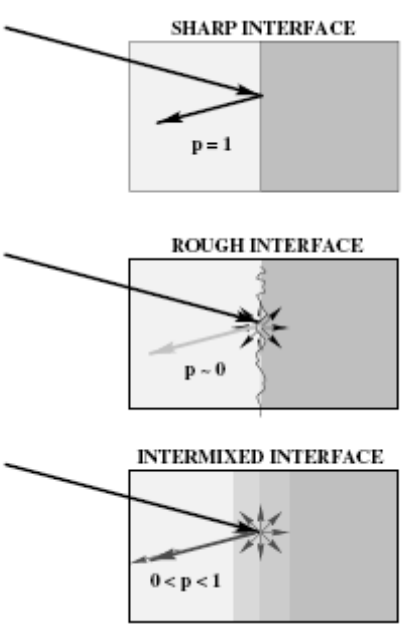

Figure 11. A schematic presentation of the value of *p* for three different cases.

$$H(t,\phi) = 1 + \frac{\beta}{\cos\phi \times \left(1 - \frac{1}{t^2}\right)^{1/2}} \qquad (11)$$

where *d* is the total multilayer thickness.

The high resistivity of the pristine sample now can be attributed to the two parameters – *R* and *p*. Since in most practical cases the as-deposited thin films/multilayers have rough interfaces, the value of *p* for the pristine sample can be fixed to zero. One now has to adjust the value of *R* to reproduce the experimental resistivity and then verify whether this value seems logical. Numerical solution of Eqns. (7) – (11), when adjusted to reproduce the experimental resistivity, yields R = 0.66. Here, *D* values have been taken as the grain sizes determined by the Scherrer's method applied to the XRD data, and the electron mean free paths in *Fe* and *Ni* have been taken as 20 nm and 12 nm, respectively[29]. The value of *R* for metal thin films has been shown to be in the range 0.30 – 0.80[25], and hence the *R*=0.66, determined for our pristine sample, is quite reasonable.

The resistivity after 1×10^{13} ions/cm^2 irradiation drops down to half of its pristine value (Fig. 10). The clue for this drop can be taken from the XRD data, which shows an interface mixing of about 20 per cent at this fluence. The irradiated multilayer, therefore, can be modelled as having the pristine layer structure with an increased specular scattering component *p* (Fig. 11). The thick arrows represent the directions of electrons before and after scattering from the interface. The group of thin small arrows is a representative of diffuse scattering. The darkness of the arrows shows the intensity of scattering. At a sharp interface, there is pure specular scattering of electrons yielding *p* = 1. While, a rough interface acts as a centre of strong diffuse scattering and the specularity approaches zero. In the case of an intermixed interface, however, the strength of the diffuse scattering becomes low and the specularity assumes a value between 0 and 1. By taking the internal defect and grain boundary structure the same (*R* = 0.66) after irradiation as a crude approximation, the resistivity at this fluence requires *p* to be equal to 0.65 – a highly smoothened interface consistent with the XRD results. The augmentation to 1×10^{14} ions/cm^2 fluence of irradiation leads to a further drop in the resistivity to 23.2 μΩ-cm (Fig. 10). One needs to look back once again at the corresponding XRD data, which suggests an almost complete mixing of *Fe* and *Ni* layers at this fluence – the multilayer structure has been broken, the interfaces removed, and the presumably uniform composite now has a thickness *d* = 46 nm, the total initial multilayer thickness. This composite layer is now thicker than the corresponding electron mean free path – an average of the values in *Fe* (20 nm) and *Ni* (12 nm) – and hence the layer resistivity should be equal to the bulk resistivity of the composite. The composite–consisting of ~65% *FeNi* and ~35 % $FeNi_3$ phases as observed from the XRD–should have the resistivity ρ_∞, *Fe*-*Ni* equal to ~23 μΩ-cm, which is the same as that of the 1×10^{14} ions/cm^2 irradiated sample.

Thus, the XRD and resistivity measurements, show independently as well as in mutual agreement that SHI's can produce mixing also in metal/metal systems and that

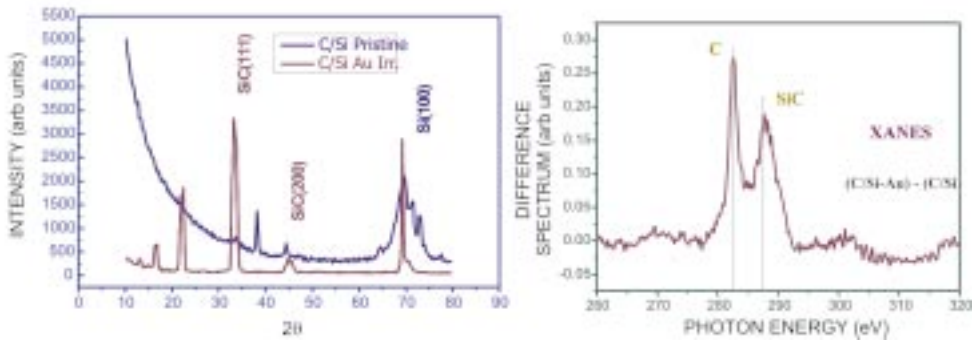

(a) **(b)**

Figure 12. (a) XRD and (b) XANES different spectra for the pristine and 120 MeV, 1×10^{13} ions/cm^2 irradiated *C*/*Si* multilayers.

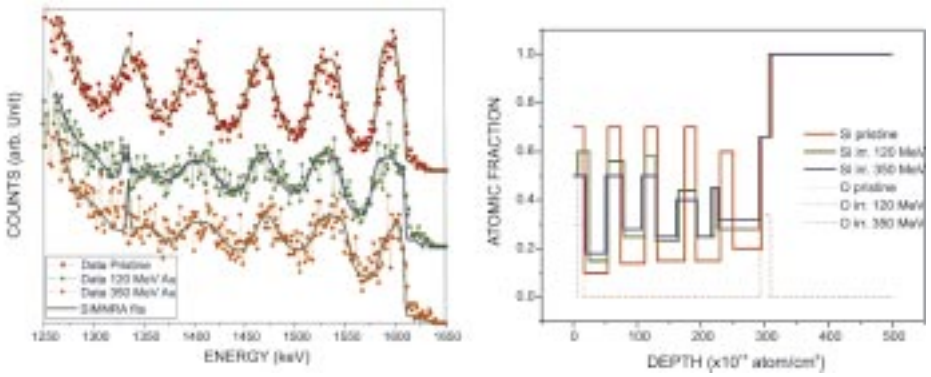

Figure 13. (a) HRBS spectra of pristine and 1×10^{14} ions/cm^2 120 and 350 MeV *Au* irradiated C_{60}/*Si* multilayers. The experimental data are shown by symbols + broken lines; the continuous lines are the corresponding SIMNRA fits. The base lines of the three spectra are shifted along the y-axis for better clarity. (b) Step-function depth profiles for the multilayers according to the fit values from the SIMNRA simulations.

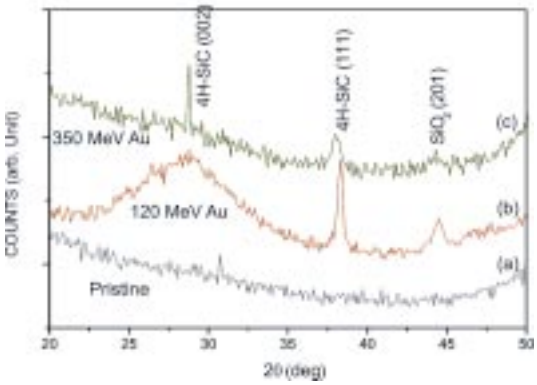

Figure 14. XRD spectra of pristine and 1×10^{14} ions/cm^2 120 and 350 MeV *Au* irradiated C_{60}/*Si* multilayers.

the processes based on the thermal spike model can be attributed for SHI mixing.

2.5 C-allotrope/*Si* Multilayer: *SiC* Formation at Room Temperature

At this juncture, when the mechanism of SHI mixing is understood to a considerable extent, it is quite intriguing to exploit it to synthesize thin films of materials of technological importance. In this regard, silicon carbide qualifies as an appropriate material. Currently, there is an increasing drive to reduce the synthesis temperature of thin *SiC* films, which have alluring superior properties, mainly their wide-band-gap semiconductivity and excellent thermal, chemical and corrosional stability. *SiC* thin films are being grown by several different processes, but all of them require a high temperature (>1000 °C) at some stage, which restricts their application to device fabrication processes capable of withstanding such temperatures. The ultimate goal would be to bring the synthesis temperature down to room temperature (RT). In the light of the requirement of very high *Si*-*C* reaction temperatures, SHI's seem to be quite appropriate, for the production of high temperature conditions by SHI's is more or less established by now. One would thus expect that SHI mixing at RT of multilayers of some *C*-allotropes and *Si* might yield crystalline *SiC* without heat treatment. As an attempt in this direction, we devised 120 MeV and 350 MeV *Au* ion irradiations of [*a*-C (15 Å)/*Si* (30 Å)]×8 and [C_{60} (45 Å)/*Si* (30 Å)]×5 multilayers deposited on *Si* substrates and characterization by XRD, X-ray absorption near-edge spectrometry (XANES), and HRBS[30,31].

The XRD and XANES spectra for the 120 MeV, 1×10^{13} ions/cm^2 irradiated C/*Si* multilayers are shown in Fig. 12. As revealed by the XRD spectra, the pristine film exhibits amorphous nature, and the structure at interface is complex close to the *Si* substrate. After irradiation, new and sharp reflections, indicative of the presence of crystalline material, appear. The reflections at ~33.5° and ~45° correspond to *Si* (111) and *Si* (200) planes, respectively. The degree of crystallinity of *SiC* islands varies considerably, and the predominantly (111) oriented *SiC* grains possess cubic lattice structure, commonly known as β-*SiC*. The normalised difference XANES spectrum also exhibits a *SiC* peak, indicative of formation of the phase after irradiation.

Figure 13 shows the HRBS spectra and corresponding SIMNRA fits for the pristine and 120 and 350 MeV, 1×10^{14} ions/cm^2 irradiated C_{60}/*Si* multilayers. The spectrum of the pristine sample exhibits well-separated peaks and thereby shows the good quality of the multilayer. After irradiation, a significant smearing out of these peaks, is observed for both the ion energies, indicating an intermixing of *Si* and *C* atoms at the interfaces. The approximate, step-function depth-profiles as derived from the SIMNRA fits are also shown in Fig. 13. These depth profiles enable one to readily conclude that SHI irradiations have induced considerable intermixing at the C_{60}/*Si* interfaces. Furthermore, the XRD spectra, as shown in Figure 14, reveal the formation of crystalline 4H-*Si*C phases in the C_{60}/*Si* multilayers after irradiation.

In essence, SHI mixing technique is capable of synthesising at RT the crystalline *Si*C phases, which otherwise require very high temperatures.

3. SUMMARY

The underlying mechanism of SHI mixing across interfaces is discussed and some experimental proofs, which lead to

the present day understanding of the subject, are presented. It is argued that the thermal spike model of SHI-matter interaction is applicable in the case of SHI mixing. The process is shown to be capable of producing high temperature phases, thus validating the applicability of the model. The hypothesis that SHI mixing is a consequence of transient molten state diffusion is proved via a thorough and careful analysis of an *Fe*/*Si* mixing experiment. A thermodynamical parameter, viz., interfacial free energy, is shown to play a role in determining the extent of mixing. The SHI mixing process has been demonstrated to take place also in a metal/metal system, wherein the thermal spike model is valid exclusively. The findings have been exploited to synthesise *Si*C at RT via SHI mixing of C-allotrope/*Si* multilayers.

ACKNOWLEDGEMENTS

The authors wish to acknowledge all those who supported and participated in performing the experiments and shaping up the ideas presented in the paper. In particular, they are grateful to Prof Ajay Gupta, UGC-DAE CSR, Indore; Dr W. Assmann, LMU, München; Prof Dr. H.D. Carstanjen, MPI-MF, Stuttgart, Dr M. Toulemonde, CIRIL-Caen, and Dr B. Schattat, Universität Stuttgart for their support, advice, encouragement, and guidance.

REFERENCES

1. Thibaudau, F.; Cousty, J.; Balanzat, E. & Bouffard, S.Atomic-force-microscopy observations of tracks induced by swift Kr ions in mica. *Phys. Rev. Lett.* 1991, **67,** 1582-585.
2. Barbu, A.; Dunlop, A.; Lesueur, D. & Averback, R.S.Latent Tracks Do Exist in Metallic Materials. *Europhys. Lett.* 1991, **15**, 37-42.
3. Dufour, C.; Bauer, Ph.; Marchall, G.; Grilhe, J.; Jaounen, C.; Pacaud, J. & J. C. Jousset, J. Ion Beam Mixing Effects Induced in the Latent Tracks of Swift Heavy Ions in a Fe/Si Multilayer. *Europhys. Lett.* 1993, **21,** 671-78.
4. Klaumünzer, S.; Ming-dong Hou, & Schumacher, G.Coulomb Explosions in a Metallic Glass Due to the Passage of Fast Heavy Ions. *Phys. Rev. Lett.* 1986, **57,** 850-53.
5. Wang, Z. G.; Dufour, C.; Paumier, E. & Toulemonde, M.The Se sensitivity of metals under swift-heavy-ion irradiation: a transient thermal process. *J. Phys.: Condens. Matter.* 1994, **6**, 6733-750.
6. Gupta, Ajay & Avasthi, D. K. Large electronically mediated sputtering in gold films. *Phys. Rev.* 2001, B **64**, 155407.
7. Toulemonde, M.; Assmann, W.; Trautmann, C. & Grüner, F. Jetlike Component in Sputtering of LiF Induced by Swift Heavy Ions. *Phys. Rev. Lett.* 2002, **88**, 057602-057605.
8. Schiwietz, G.; Xiao, G.; Luderer, E.& Grande, P. L. Auger electrons from ion tracks. *Nucl. Instrum. Methods Phys. Res.* B **164–165**, 353-64.
9. Srivastava, S.K.; Ghosh, S.; Gupta, A.; Ganesan, V.; Assmann, W.; Kruijer, S. & Avasthi, D.K. Conversion Electron Mössbauer Study of Mixing Induced by Swift Heavy Ions at the Fe/Si Interface, *Hyperfine Interactions.* 2001, **133,** 53-57.
10. Srivastava, S.K. Synthesis of Compounds and Nanophases by Swift Heavy Ions, Inter-University Accelerator Centre (Formerly Nuclear Science Centre), New Delhi, Aug. 2002. Ch. 4, Ph D thesis.
11. Assmann, W.; Dobler, M.; Avasthi, D.K.; Kruijer, S.; Mieskes, H.D. & Nolte, H.Swift heavy ion induced formation of α-$FeSi_2$. *Nucl. Instr. Meth. Phys. Res.* 1998, B **146**, 271-77.
12. Srivastava, S.K.; Avasthi, D.K.; Assmann, W.; Wang, Z.G.; Kucal, H.; Jacquet, E.; Carstanjen, H.D. & Toulemonde, M.Test of the hypothesis of transient molten state diffusion for swift-heavy-ion induced mixing. *Phys. Rev.* 2005, B **71**, 193405-3408.
13. Mayer, M. MPI für Plasmaphysik, Garching, Germany, Report No. IPP 9/113, 1997 (unpublished).
14. Toulemonde, M.; Dural, J.; Nouet, G.; Mary, P.; Hamet, J.F.; Beaufort, M.F.; Desoyer, J.C.; Blanchard, C. & Auleytner, J. High Energy Heavy Ion Irradiation of Silicon. *Phys. Status. Solidi.* 1989, A **114,** 467-73.
15. Wang, Z.G.; Dufour, C.; Euphrasie, S. & Toulemonde, M. Electronic thermal spike effects in intermixing of bilayers induced by swift heavy ions. *Nucl. Instr. Meth. Phys. Res.* 2003, B **209**, 194-99.
16. Gaiduk, P.I.; Larsen, A.N.; Hansen, J.L.; Wendler, E. & Wesch, W. Temperature effect on defect evolution in 800 keV Ge-implanted Si/SiGe multi-layered structure. *Physica.* 2003, B **340-342**, 813-17.
17. Guillemot, F.; Thibon, I.; Dibuigue, J. & Ansel, D. Calculations of Interdiffusion Coefficients via an Extended Boltzmann-Matano Analysis of the Ti-Mo-Ta System. *Defect Diffus. Forum*. 2001, **194-197**, 247-52.
18. Gibbs, K.M.; Brown, W.L. & Johnson, R.E. Electronic sputtering of condensed O_2. *Phys. Rev.* 1988, B **38,** 11001-1007.
19. Arnoldbik, W.M.; Tomozeiu, N. & Habraken, F.H.P.M. Electronic sputtering of thin SiO2 films by MeV heavy ions *Nucl. Instr. Meth. Phys. Res.* 2003, B **203,** 151-57.
20. deWijs, G.A.; Kresse, G.; Vocadlo, L.; Dobson, D.; Alfe, D.; Gilan, M.J. & Price, G.D. The viscosity of liquid iron at the physical conditions of the Earth's core, *Nature* (London). 1998, **392,** 805-06.
21. Yu, W.; Wang, Z.Q. & Stroud, D.Empirical molecular-dynamics study of diffusion in liquid semiconductors. *Phys. Rev.* 1996, B **54**, 13946-3954.
22. Borg, R.J. & Lai, D.Y.F. Diffusion in α -FeSi Alloys. *J. Appl. Phys.* 1970, **41**, 5193-200.
23. Clemens, B.M. & Hufnagel, T.G. Amorphous alloys formed by solid state reaction. *J. Alloys Compd.* 1993, **194**, 221-27.
24. Clemens, B.M.Solid-state reaction and structure in compositionally modulated zirconium-nickel and titanium-

nickel films. *Phys. Rev.* 1988, B **33,** 7615-624.
25. Srivastava, S.K.; Kumar, R.; Kabiraj, D.; Patel, R.S.; Majumdar, A.K.; Gupta, A. & Avasthi, D.K. Swift heavy ion induced mixing in Fe/Ni multilayer. *Nucl. Instr. Meth. Phys. Res. B*, 2006, **243**, 304-312.
26. Fuchs, K. The conductivity of thin metallic films according to the electron theory of metals. *Mathematical Proceedings of the Cambridge Philosophical Society*, 1938, **34**, 100-108.
27. Mayadas, A.F. & Shatzkes, M. Electrical-resistivity model for polycrystalline films: the case of arbitrary reflection at external surfaces. *Phys. Rev. B*, 1970, **1**, 1382-1389.
28. Zhang, X.–G. & Butler, W.H. Conductivity of metallic films and multilayers. *Phys. Rev. B*, 1995, **51**, 10085-10103.
29. Maissel, L.I. & Glang, R. Handbook of Thin Film Technology, McGraw-Hill, New York, 1970.
30. Asokan, K.; Srivastava, S.K.; Kabiraj, D.; Jan, J.C.; Pong, W.F.; Mookerjee, S. & Avasthi, D.K. Study of ion beam mixing in C/Si multilayers by X-ray absorption spectroscopy. *Nucl. Instr. Meth. Phys. Res. B*, 2002, **193**, 324-328.
31. Srivastava, S.K.; Kabiraj, D.; Schattat, B.; Carstanjen H.D. & Avasthi, D.K. Swift heavy ion induced modification of Si/C_{60} multilayers. *Nucl. Instr. Meth. Phys. Res. B*, 2004, **219-220**, 815-819.

Contributors

Dr Sanjeev Kumar Srivastava did his PhD in Materials Science from Inter University Accelerator Centre, New Delhi in 2002. He is currently an Assistant Professor in the Department of Physics and Meteorology of the IIT Kharagpur. He acquired specialization in Swift Heavy Ion based Materials Engineering and Characterization, Nuclear Condensed Matter Physics, Local Magnetism, Quantum Criticality, and ab-initio DFT calculations of electronic properties of solids. He spent two years in the MPI für Metallforschung, Stuttgart, Germany and has to his credit 26 publications in national/international journals and 8 such in conference proceedings.

Dr Devesh Kumar Avasthi (*See page* 362)